Competition between one- and two-photon processes in Ar irradiated by the Shanghai soft x-ray free electron laser

Ruichao Dong,[1,2,7,*] Jie Yan,[3,4,*] Jinze Feng,[2] Mingjie Zhang,[1,7] Yikang Zhang,[2] Yuliang Guo,[2] Ahai Chen,[2] Zhenjie Shen,[2] Yuneng Shen,[2] Zhen Wang,[1] Kaiqing Zhang,[1] Xuan Li,[1] Zheng Qi,[1] Zhangfeng Gao,[1] Zenggong Jiang,[1] Jiaming Jiang,[2] Bin Li,[1] Chao Feng,[1] Bo Liu,[1] Huaidong Jiang,[2] Zhi Liu,[2] Yajiang Hao,[5] Kiyoshi Ueda,[2,8] Cheng Gao,[4,†] Xincheng Wang,[2,‡] and Yuhai Jiang[2,6,1,§]

[1]*Shanghai Advanced Research Institute, Chinese Academy of Sciences, Shanghai 201210, China*

[2]*Center for Transformative Science and School of Physical Science and Technology, ShanghaiTech University, Shanghai 201210, China*

[3]*Shanghai EBIT Laboratory, Key Laboratory of Nuclear Physics and Ion-Beam Application (MOE), Institute of Modern Physics, Fudan University, Shanghai 200433, China*

[4]*Department of Physics, College of Science, National University of Defense Technology, Changsha, Hunan 410073, China*

[5]*Institute of Theoretical Physics and Department of Physics, University of Science and Technology Beijing, Beijing 100083, China*

[6]*School of Physics, Henan Normal University, Xinxiang 453007, China*

[7]*University of Chinese Academy of Sciences, Beijing 100049, China*

[8]*Department of Chemistry, Tohoku University, Sendai 980-8578, Japan*

(Received 25 February 2025; accepted 29 July 2025; published 21 August 2025)

Shanghai Soft X-ray Free Electron Laser facility has entered user operation, delivering soft x-ray pulses in self-amplified spontaneous emission mode with an intensity of the peak fluence of $\sim 1.0 \times 10^{-2}$ μJ/μm^2 at a focus point. With these conditions, at a photon energy of 260 eV, we expect sequential processes in which Ar^{2+} created by the Auger decay following the $2p$ photoionization may be resonantly excited to the $2p^{-1}3p^{-2}3d$ inner-shell excited state and thus resonant Auger decay produces Ar^{3+}, which can also be competitively produced by the direct double Auger decay (DDAD) following the one-photon $2p$ ionization of Ar. Ar^{4+} ions dominantly arise from Ar^{2+} with a resonant excitation and subsequent DDAD, involving two-photon absorption. The measured charge distributions as a function of the free-electron laser (FEL) fluence are well reproduced by *ab initio* calculations that include DDAD, normally neglected in the previous FEL studies, and resonant Auger decay. The present results demonstrate that the low peak fluence of the FEL pulses can be determined if the competition between the one- and two-photon processes is precisely described along with DDAD and resonant Auger decay.

DOI: 10.1103/j4rx-55m2

Shanghai Soft X-ray Free Electron Laser Facility (SXFEL) [1], the first x-ray free-electron laser (XFEL) in China, provides short, intense, and transversely coherent x-ray pulses in the energy range 100–620 eV in the self-amplified spontaneous emission (SASE) mode. The development of XFELs has provided unique opportunities to investigate the structure and dynamics of various systems ranging from atoms and molecules to bioparticles [2–6]. The SXFEL is composed of a 1.5 GeV linear accelerator, two undulator lines with two beamlines each, and five endstations in Phase I. As one of the five endstations, the Atomic, Molecular and Optical Sciences (AMO) endstation provides a tool to study the fundamental processes of matter irradiated with ultraintense femtosecond x-ray.

When intense XFEL pulses are irradiated on atoms, various electronic processes, such as photoionization, resonant excitation (RE), and Auger decay, may occur sequentially as the atoms reach highly charged states [7,8], and they are highly sensitive to the photon energy and fluence of x-rays. In these sequential processes, the absorption of a few photons and the emission of some electrons are involved, and complex many-body interactions and electron correlations may play an essential role [9–11]. As one of the crucial processes in the highly nonlinear regime, transient resonances provide interaction strengths more than 1000 times greater than those in the continuum and allow selective manipulation of quantum states [12,13]. Previous studies [14–16] have shown that resonance-enabled x-ray multiple ionization is an efficient way for atoms to reach high charge states. Auger decay is another important process that typically occurs after the creation of an inner-shell hole in an atom, leading to the release of electrons with the characteristic energy [17–20]. Except for the well-known single Auger decay (SAD), it is also known

*These authors contributed equally to this work.
†Contact author: gaocheng@nudt.edu.cn
‡Contact author: wangxch1@shanghaitech.edu.cn
§Contact author: jiangyh3@shanghaitech.edu.cn

Published by the American Physical Society under the terms of the Creative Commons Attribution 4.0 International license. Further distribution of this work must maintain attribution to the author(s) and the published article's title, journal citation, and DOI.

that inner-shell holes may de-excite by emitting two Auger electrons [21,22]. These two electrons can be emitted either simultaneously via a direct double Auger decay (DDAD) or sequentially through a cascade double Auger decay process, where electron-electron correlations need complicate electron release dynamics [23–25]. The DDAD normally assumed with a much lower probability, omitted in the previous FEL studies, is still competitive if the SAD followed by RE needs one more photon.

As pulse fluence is one of the most critical parameters in free-electron laser (FEL) experiments, its absolute measurement is imperative to elucidate the underlying physics of the generation processes and to enhance data analysis. For the extreme ultraviolet wavelength range, the pulse energy of FEL can be accurately measured using gas monitor detectors [26]. The development of the latest x-ray gas monitor extends this operation range to hard x-ray photon energies of up to 30 keV [27]. Another methodology employs gas detectors and multipliers for relative fluence measurements, where absolute fluence is established through sensor-based conditional triggers and algorithms [28]. Although both methods are effective for measuring average pulse energy, they do not provide peak fluence measurements at the interaction point. Recent advances in theoretical methods [29–31], combined with experimental data, have facilitated precise evaluations of pulse peak fluence at the interaction point for high- to moderate-fluence XFELs. Nevertheless, accurate measurement of the relatively low peak fluence in the soft x-ray region, resulting in absorption of only a couple of photons at the interaction point, still remains a challenge. With specific photon energy, *ab initio* calculations for determining the low peak fluence can be established by studying reaction channels that are highly sensitive to the XFEL intensity, such as the competition between one-photon DDAD and two-photon RSAD (resonant SAD), followed by resonant absorption of a second photon.

In this article, the multiple ionization mechanism of Ar atoms is investigated by initiating ionization with photon energy of 260 eV, which exceeds the Ar $2p$ ionization threshold of 246.5 and 248.6 eV, but below the Ar^+ $2p$ ionization threshold of 262.5 eV. It is found that the two-photon RSAD and one-photon DDAD processes significantly influence the charge state distributions (CSDs) of the Ar ions. Using an *ab initio* model that incorporates two-photon RSAD and one-photon DDAD processes, we reproduce the peak fluence-dependent ion yields and demonstrate competition between one- and two-photon processes. Furthermore, with the precise theoretical framework, the peak fluence of XFEL pulses at the interaction point can be determined, even for relatively low fluence pulses, which is hardly accessible with other diagnostic tools.

The experiment was performed at the AMO endstation of the SXFEL, using SASE x-ray pulses generated by the undulator line in Phase I. The 260 eV x-ray pulses produced with a bandwidth of less than 1%, a pulse energy of ∼10 μJ, and a repetition rate of 4 Hz are reflected by a plane mirror before an online variable line-spacing grating, the zeroth order of which is focused on the interaction point of the reaction microscope [32–34] by an ellipsoidal mirror. The x-ray pulse duration and focus size are estimated to be 100 fs (FWHM) and ∼20 × 20 μm^2, respectively. The Ar gas jet, generated by supersonic expansion from a 50 μm nozzle with an injection pressure of 5 bar is collimated by two skimmers with diameters of 0.2 and 0.4 mm, respectively, before flowing into the intersection region. The ions generated in the x-ray–Ar interaction area are extracted by a homogeneous electrostatic field of 5 V/cm toward a microchannel plate (MCP) detector equipped with delay-line anode. The XFEL beam is dumped into a Faraday cup, which provides the relative XFEL pulse energy on an event-by-event basis.

A typical time-of-flight spectrum is presented in Fig. 1(a); Ar^{z+} ions with charge states up to $z = 4$ can be observed. It is obvious that the generation of doubly charged Ar^{2+} is dominated. This can be understood through the transition pathways indicated in Fig. 1(b). For Ar in the ground configuration ($1s^2 2s^2 2p^6 3s^2 3p^6$), the liberation of a $2p$ electron during the interaction with 260 eV photon is dominating. The $2p$ core-hole states are inherently unstable, so that electronic relaxation through Auger decay will eventually lead to Ar^{2+}. However, the production of Ar^{3+} is competing in the presence of two possibilities. One possible path is the relaxation of the $2p$ core-hole state through one-photon DDAD, which has been observed in previous studies [35,36]. Alternatively, a resonance absorption of one more XFEL photon will lead to $2p^{-1}3p^{-2}3d$, i.e., $3p^{-2} + h\nu \rightarrow 2p^{-1}3p^{-2}3d$, and then sequentially to reach Ar^{3+} followed by SAD, i.e., two-photon RSAD. The competition between the two pathways—one-photon DDAD and two-photon RSAD processes—can be further demonstrated by the fluence-dependent CSD analyses. Furthermore, it is found that the formation of Ar^{4+} ions is predominantly from two-photon RDDAD (resonant DDAD) of $2p^{-1}3p^{-2}3d$ states in the low fluence of the XFEL beam, as characterized in the following analysis.

To understand reaction mechanisms in detail, a time-dependent rate equation (TDRE) method [37–39] based on the fine-structure level approximation is utilized. The population evolution of atomic state n_i is determined by the following rate equation:

$$\frac{dn_i}{dt} = \sum_{j\neq i}^{N_L} n_j R_{ji} - n_i \sum_{j\neq i}^{N_L} R_{ij}, \tag{1}$$

where N_L represents the total number of energy levels considered in the calculation, and R_{ij} and R_{ji} denote the microscopic atomic rates of transitions $i \rightarrow j$ and $j \rightarrow i$, respectively. In this work, when the liberated electrons from x-ray–Ar interaction escape easily, atomic processes caused by electron collisions are omitted in constructing the rate equations, while photoexcitation, radiative decay, photoionization, SAD, and RSAD are explicitly included. Specifically, DDADs induced by one and two photons are also incorporated using our recently developed methods [40–43], which play an important role in CSDs. The details of the TDRE were addressed in Refs. [37–39].

To construct the rate equations, we calculate a comprehensive set of atomic data for Ar-Ar^{5+}, including energy levels, radiative decay rates, photoionization cross sections, and Auger decay rates (see the Supplemental Material for details [44]). For the Ar atom, only the ground-state configuration is considered, while for other Ar ions, both the ground and singly excited configurations from valence

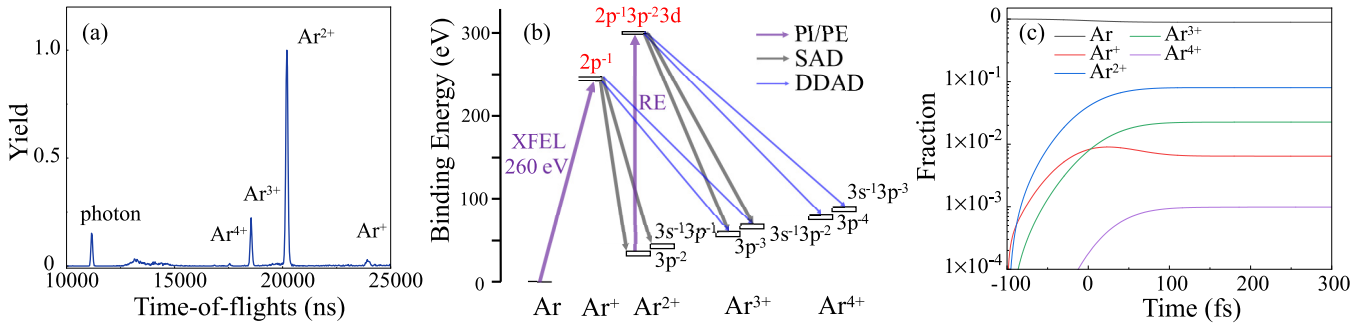


FIG. 1. (a) Time-of-flight spectrum of Ar with XFEL pulses at 260 eV. (b) Dominant pathways of Ar irradiated by the XFEL pulse: photoionization/excitation (PI/PE), SAD, DDAD, and RE. (c) Theoretical population evolution of Ar-Ar^{4+} at the peak fluence of 1.0×10^{-2} μJ/μm^2 (see later) and the pulse duration of 100 fs (FWHM). The XFEL pulse intensity reaches its maximum at $t = 0$ fs.

shells are included. In particular, excited configurations from the $2p$ orbital are also taken into account. Taking Ar^{2+} as an example, the following configurations are examined: [He] $L^8 3s^2 3p^4$, $L^8 3s^2 3p^3 3d$, $L^8 3s 3p^5$, $L^8 3s 3p^4 3d$, $L^7 3s^2 3p^5$, $L^7 3s 3p^6$, $L^7 3s^2 3p^4 3d$, $L^6 3s^2 3p^6$, and $L^6 3s^2 3p^5 3d$, where L^m means m electrons randomly occupying L shell. The calculations are performed using the flexible atomic code [45], which is based on the multiconfiguration Dirac-Hartree-Fock approximation. The good agreement between theoretical predictions and synchrotron radiation results validates the accuracy of our model [20,46] (see the Supplemental Material for details [44]).

In this work, x-rays are used to ionize a $2p$ electron in the Ar atom, creating a $2p$ hole. Utilizing a comprehensive set of atomic data, we calculated the rates of relevant atomic processes. The calculated Auger decay rate for the $2p^{-1}$ state is around 1.8×10^{14} s^{-1}, while the DDAD rate is approximately 2.5×10^{13} s^{-1}, consistent with experimental findings [47]. In contrast, the triple Auger decay rate is significantly weaker [36,48] and thus negligible. This rapid decay leads to near-instantaneous filling of $2p^{-1}$ vacancies upon their creation.

By solving rate equations, the temporal evolution of atomic states can be obtained. A Monte Carlo algebra is developed to accelerate the calculation [43,49,50]. The details of Monte Carlo can be found elsewhere [43]. In brief, we track the states' evolution of Ar atoms and obtain level populations by statistics. Initially, the Ar atom is populated in its ground state ($1s^2 2s^2 2p^6 3s^2 3p^6$). From the initial state, we calculate the transition probabilities for all possible transition channels. We randomly choose the channel through which the atom would go. Consequently, the final state determined is set to be the initial state for the next time step. Such procedures are repeated until the tracked atom has no way to go, and so we get a sample. The level populations are obtained by statistics for enough samples. In this work, more than 10^8 samples are simulated to a convergent result. We set the laser intensity to reach its maximum at $t = 0$ fs. The simulation starts from -100 fs and ends at 9900 fs.

The temporal population evolution of different charge states of Ar is shown in Fig. 1(c). Due to the high Auger decay rate, the population of Ar^{2+} rapidly increases and Ar^{2+} becomes the dominant ionization stage after 10 fs. As the x-ray intensity reaches its maximum ($t = 0$ fs), the population fraction of Ar^{3+} starts to overtake Ar^+. The population of Ar^+ reaches its maximum around $t = 0$ fs and then decreases. Ar^{4+} is populated much later. Beyond $t = 100$ fs, the populations of Ar-Ar^{4+} are stable.

Figure 2 presents two sets of experimental CSDs for low and high peak fluence, based on the relative pulse energy measured by a Faraday cup. Two absolute values of peak flu-

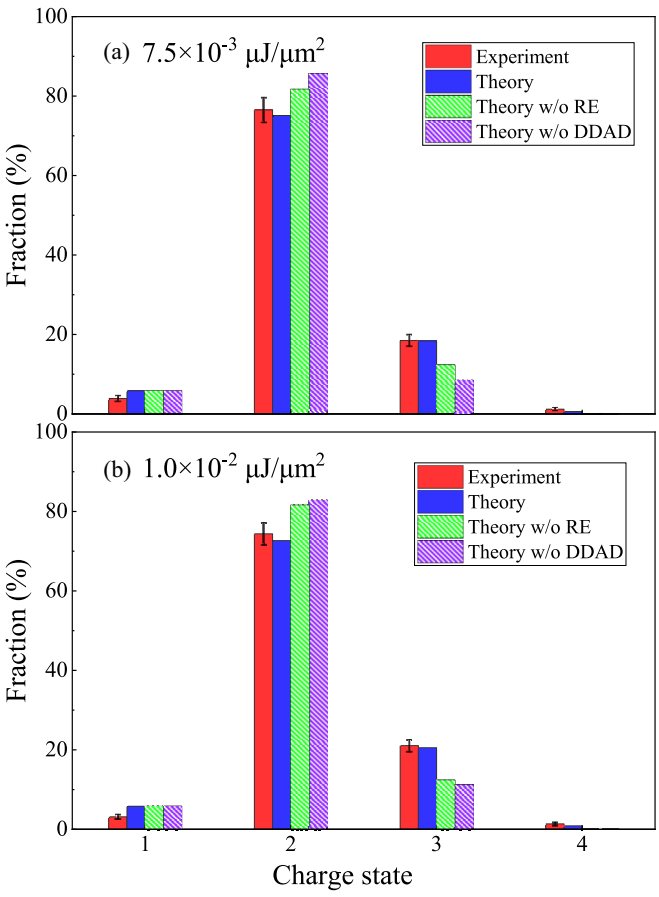


FIG. 2. The experimental CSDs (red bars) of Ar compared with theoretical calculations obtained at the peak fluence of (a) 7.5×10^{-3} μJ/μm^2 and (b) 1.0×10^{-2} μJ/μm^2. The blue bars denote theoretical predictions considering all interaction channels. The results without considering RE are shown in green and those without considering DDAD are shown in purple.

ence are determined to be 7.5×10^{-3} and 1.0×10^{-2} μJ/μm^2, respectively, by optimizing the agreement of theoretical time-integrated CSDs (blue bars) and experimental data (red bars). Experimentally, Ar^{2+} is predominantly populated, accounting for ∼76.5%. Ar^{3+} accounts for about 18.5%, and only about 1.2% is populated on Ar^{4+}. Our results show a higher proportion of highly charged ions (Ar^{3+} and Ar^{4+}) than in synchrotron radiation experiments [20,46], demonstrating the important role of two-photon processes. To reproduce the experimental results, it is essential to consider both one- and two-photon processes carefully. For instance, at low peak fluence (7.5×10^{-3} μJ/μm^2), as shown in Fig. 2(a), the population fraction of Ar^{2+} increases by about 6% if we consider only one-photon absorption, i.e., closing the RE channels in Ar^{2+}. This, in turn, decreases the population fraction of Ar^{3+} by about 6%. Furthermore, Ar^{4+} is hardly created without two-photon processes, as shown in Fig. 2(b). DDADs also play a dominant role in CSDs in both the one- and two-photon processes. If we close the DDAD channels, the population fraction of Ar^{2+} increases by about 10%, and the population of Ar^{3+} decreases significantly, while Ar^{4+} is barely creat

The characteristics at higher x-ray fluence (1.0×10^{-2} μJ/μm^2), as shown in Fig. 2(b), are similar to those at low fluence. However, the rate of RE increases as the laser fluence increases. When RE channels are closed, the population of Ar^{2+} increases by about 8%, comparable to the influence of the DDAD processes. This highlights the importance of resonant absorption in atom-XFEL interactions. Only by considering all possible interaction channels, the calculations can achieve good agreement with the experiment. This underscores the necessity of accounting for both one-photon DDAD and two-photon RSAD processes to accurately describe the ionization dynamics of Ar in XFEL fields.

In order to further demonstrate the competition between one-photon DDAD and two-photon RSAD processes in determining CSDs, we plot the ion yields as a function of the XFEL peak fluence in Fig. 3. Experimental peak fluence in Fig. 3 is calibrated using optimized values from all data sets, including the two sets shown in Fig. 2. Considering all physical processes [Fig. 3(a)], the slopes of the population in Ar^+ and Ar^{2+} are approximately 0.9, indicating that these ions are primarily produced by absorption of one photon. The theoretical slopes for Ar^+ and Ar^{2+} are not equal to 1 due to computational uncertainties and saturation effects at higher peak fluence. We also note that experimental Ar^+ ions are detected obviously lower than theoretical predictions, which is due to the detection efficiency and the depletion of the MCP. In contrast, the slope for Ar^{4+} is around 1.9, signifying its dominant production through two-photon absorption [refer to Fig. 1(b)]. The population slope of Ar^{3+} is measured at 1.3, reflecting the competition between one- and two-photon processes, as demonstrated in Fig. 2. If the RE processes are excluded [Fig. 3(b)], the slope of Ar^{3+} decreases to 1, as it is produced solely through one-photon processes and consequently results in minimal formation of Ar^{4+}. Conversely, if we exclude the DDAD processes [Fig. 3(c)], Ar^{3+} is predominantly populated through two-photon absorption, with the population slope approaching 1.8. The population of Ar^{4+} remains much lower than measurements, as it is primarily produced by two-photon RDDAD from Ar^{2+}. One can note

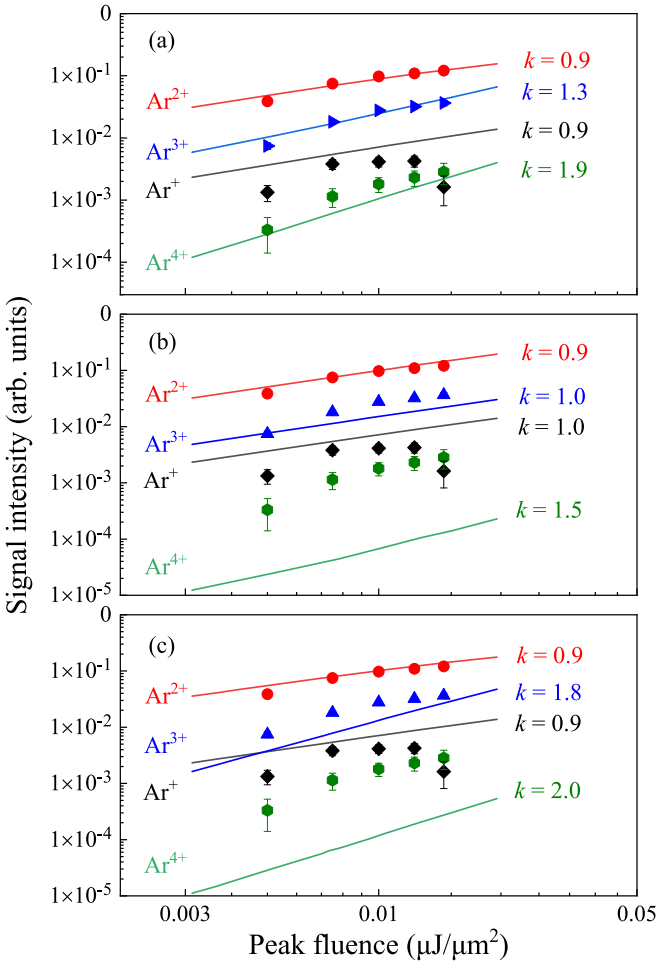


FIG. 3. Ion yields as a function of the XFEL peak fluence. Experimental data points for Ar^+ (black diamonds), Ar^{2+} (red circles), Ar^{3+} (blue triangles), and Ar^{4+} (olive diamonds), compared with theoretical simulations (solid lines). In panel (a), all channels are considered in theoretical predictions. RE processes are not considered in panel (b) and DDAD processes are not considered in panel (c). The numbers indicate the slope of the populations of Ar ions.

that small amounts of Ar^{4+} counts with the slopes of 1.5 and 2 in Figs. 3(b) and 3(c) are visible even if RSAD/DDAD mentioned above is not considered in calculation, resulting from other much weaker pathways, not discussed here. The CSDs as a function of the XFEL peak fluence are well reproduced by theoretical calculations that include precisely all relevant processes, further enabling to determine absolute experimental peak fluence. Finally, the peak fluence at the interaction point is determined to be $\sim 1.0 \times 10^{-2}$ μJ/μm^2 [$(0.5–1.5) \times 10^{-2}$ μJ/μm^2; see Fig. 3]. The peak intensity is estimated to be around 1×10^{13} W/cm^2 based on a pulse duration of 100 fs, which is consistent with the peak fluence estimated in our experiment ($\sim 3.2 \times 10^{13}$ W/cm^2).

In summary, we investigated the competitive dynamics of one-photon DDAD and two-photon RSAD processes induced by absorption of one and two photons in Ar atom, respectively, utilizing the new SXFEL facility and a precisely developed theoretical model. This present study demonstrates how two-photon RSAD and one-photon DDAD interact competitively

in the soft x-ray regime at 260 eV; i.e., the DDAD processes play an essential role in the creation of highly charged states. Ar^{2+} ions, primarily formed through Auger decay following $2p$ photoionization, can be resonantly excited to the inner-shell state $2p^{-1}3p^{-2}3d$, i.e., two-photon RSAD, resulting in the production of Ar^{3+}. Furthermore, Ar^{3+} can also be generated competitively via one-photon DDAD after single-photon $2p$ ionization. Meanwhile, Ar^{4+} ions predominantly arise from the RE of Ar^{2+}, followed by two-photon RDDAD, a process that requires the absorption of two photons. The experimental CSDs as a function of FEL fluence were well reproduced using *ab initio* calculations that precisely describe the competition between the one- and two-photon processes involving one-photon DDAD, two-photon RSAD, and two-photon RDDAD. The good agreement between experimental results and theoretical calculations allows us to estimate the peak fluence at the interaction point to be approximately $1.0 \times 10^{-2}\,\mu J/\mu m^2$, even at low fluence levels where only one- and two-photon processes take place. The findings not only contribute to the fundamental understanding of x-ray multiple ionization processes but also have practical implications for determining the low peak fluence of XFEL pulses.

ACKNOWLEDGMENTS

The authors acknowledge SXFEL in Shanghai, China, for the provision of XFEL beamtime at the AMO endstation and thank the facility team for their assistance and cooperation. This work was supported by the National Key Research and Development Program of China (No. 2022YFA1604302) and the National Natural Science Foundation of China (No. 12334011 and No. 12335015). We also acknowledge support from the Shanghai-XFEL beamline project (SBP) (Grant No. 31011505505885920161A2101001). K.U. acknowledges support from the CAS President's International Fellowship Initiative (PIFI).

DATA AVAILABILITY

The data that support the findings of this article are not publicly available upon publication because it is not technically feasible and/or the cost of preparing, depositing, and hosting the data would be prohibitive within the terms of this research project. The data are available from the authors upon reasonable request.

[1] B. Liu, C. Feng, D. Gu, F. Gao, H. Deng, M. Zhang, S. Sun, S. Chen, W. Zhang, W. Fang, Z. Wang, Q. Zhou, Y. Leng, M. Gu, L. Yin, Q. Gu, G. Fang, D. Wang, and Z. Zhao, The SXFEL upgrade: From test facility to user facility, Appl. Sci. (Basel) **12**, 176 (2022).

[2] Y. H. Jiang, A. Rudenko, O. Herrwerth, L. Foucar, M. Kurka, K. U. Kühnel, M. Lezius, M. F. Kling, J. van Tilborg, A. Belkacem, K. Ueda, S. Düsterer, R. Treusch, C. D. Schröter, R. Moshammer, and J. Ullrich, Ultrafast extreme ultraviolet induced isomerization of acetylene cations, Phys. Rev. Lett. **105**, 263002 (2010).

[3] J. Ullrich, A. Rudenko, and R. Moshammer, Free-electron lasers: New avenues in molecular physics and photochemistry, Annu. Rev. Phys. Chem. **63**, 635 (2012).

[4] K. Nagaya *et al.*, Ultrafast dynamics of a nucleobase analogue illuminated by a short intense x-ray free electron laser pulse, Phys. Rev. X **6**, 021035 (2016).

[5] L. Young *et al.*, Roadmap of ultrafast x-ray atomic and molecular physics, J. Phys. B: At. Mol. Opt. Phys. **51**, 032003 (2018).

[6] C. Callegari, A. Grum-Grzhimailo, K. Ishikawa, K. Prince, G. Sansone, and K. Ueda, Atomic, molecular and optical physics applications of longitudinally coherent and narrow bandwidth free-electron lasers, Phys. Rep. **904**, 1 (2021).

[7] L. Young, E. Kanter, B. Krässig, Y. Li, A. March, T. Pratt, R. Santra, S. Southworth, N. Rohringer, L. Dimauro, G. Doumy, C. Roedig, N. Berrah, L. Fang, M. Hoener, P. Bucksbaum, J. Cryan, S. Ghimire, J. Glownia, and M. Messerschmidt, Femtosecond electronic response of atoms to ultra-intense x-rays, Nature (London) **466**, 56 (2010).

[8] P. J. Ho, C. Bostedt, S. Schorb, and L. Young, Theoretical tracking of resonance-enhanced multiple ionization pathways in x-ray free-electron laser pulses, Phys. Rev. Lett. **113**, 253001 (2014).

[9] R. Moshammer *et al.*, Few-photon multiple ionization of Ne and Ar by strong free-electron-laser pulses, Phys. Rev. Lett. **98**, 203001 (2007).

[10] A. Rudenko *et al.*, Recoil-ion momentum distributions for two-photon double ionization of He and Ne by 44 eV free-electron laser radiation, Phys. Rev. Lett. **101**, 073003 (2008).

[11] Y. Hikosaka, M. Fushitani, A. Matsuda, C.-M. Tseng, A. Hishikawa, E. Shigemasa, M. Nagasono, K. Tono, T. Togashi, H. Ohashi, H. Kimura, Y. Senba, M. Yabashi, and T. Ishikawa, Multiphoton double ionization of Ar in intense extreme ultraviolet laser fields studied by shot-by-shot photoelectron spectroscopy, Phys. Rev. Lett. **105**, 133001 (2010).

[12] E. P. Kanter *et al.*, Unveiling and driving hidden resonances with high-fluence, high-intensity x-ray pulses, Phys. Rev. Lett. **107**, 233001 (2011).

[13] A. Rörig, S.-K. Son, T. Mazza, P. Schmidt, T. M. Baumann, B. Erk, M. Ilchen, J. Laksman, V. Music, S. Pathak, D. E. Rivas, D. Rolles, S. Serkez, S. Usenko, R. Santra, M. Meyer, and R. Boll, Multiple-core-hole resonance spectroscopy with ultraintense x-ray pulses, Nat. Commun. **14**, 5738 (2023).

[14] W. Xiang, G. Cheng, Y. Fu, J. Zeng, and J. Yuan, Inner-shell resonant absorption effects on evolution dynamics of the charge state distribution in a neon atom interacting with ultraintense x-ray pulses, Phys. Rev. A **86**, 061401 (2012).

[15] B. Rudek, S.-K. Son, L. Foucar, S. Epp, B. Erk, R. Hartmann, M. Adolph, R. Andritschke, A. Aquila, N. Berrah, C. Bostedt, J. Bozek, N. Coppola, F. Filsinger, H. Gorke, T. Gorkhover, H. Graafsma, L. Gumprecht, A. Hartmann, and D. Rolles, Ultra-efficient ionization of heavy atoms by intense x-ray free-electron laser pulses, Nat. Photon. **6**, 858 (2012).

[16] B. Rudek *et al.*, Relativistic and resonant effects in the ionization of heavy atoms by ultra-intense hard x-rays, Nat. Commun. **9**, 4200 (2018).

[17] S. Schippers, R. Beerwerth, L. Abrok, S. Bari, T. Buhr, M. Martins, S. Ricz, J. Viefhaus, S. Fritzsche, and A. Müller, Prominent role of multielectron processes in K-shell double and triple photodetachment of oxygen anions, Phys. Rev. A **94**, 041401 (2016).

[18] R. Beerwerth and S. Fritzsche, MCDF calculations of Auger cascade processes, Eur. Phys. J. D **71**, 253 (2017).

[19] R. Beerwerth, T. Buhr, A. Perry-Sassmannshausen, S. O. Stock, S. Bari, K. Holste, A. L. D. Kilcoyne, S. Reinwardt, S. Ricz, D. W. Savin, K. Schubert, M. Martins, A. Müller, S. Fritzsche, and S. Schippers, Near L-edge single and multiple photoionization of triply charged iron ions, Astrophys. J. **887**, 189 (2019).

[20] A. Müller, M. Martins, A. Borovik, T. Buhr, A. Perry-Sassmannshausen, S. Reinwardt, F. Trinter, S. Schippers, S. Fritzsche, and A. S. Kheifets, Role of L-shell single and double core-hole production and decay in m-fold ($1 \leqslant m \leqslant 6$) photoionization of the Ar^+ ion, Phys. Rev. A **104**, 033105 (2021).

[21] M. O. Krause, M. L. Vestal, W. H. Johnston, and T. A. Carlson, Readjustment of the neon atom ionized in the K shell by x-rays, Phys. Rev. **133**, A385 (1964).

[22] P. Zhang, J. Trester, K. Ueda, M. Han, T. Balčiūnas, and H. J. Wörner, Time-resolved multielectron coincidence spectroscopy of double Auger-Meitner decay following Xe $4d$ ionization, Phys. Rev. Lett. **132**, 083201 (2024).

[23] Y. Hikosaka, T. Kaneyasu, P. Lablanquie, F. Penent, E. Shigemasa, and K. Ito, Multiple Auger decay of the neon $1s$-core-hole state studied by multielectron coincidence spectroscopy, Phys. Rev. A **92**, 033413 (2015).

[24] J. Viefhaus, S. Cvejanović, B. Langer, T. Lischke, G. Prümper, D. Rolles, A. V. Golovin, A. N. Grum-Grzhimailo, N. M. Kabachnik, and U. Becker, Energy and angular distributions of electrons emitted by direct double Auger decay, Phys. Rev. Lett. **92**, 083001 (2004).

[25] C. Buth, R. Beerwerth, R. Obaid, N. Berrah, L. S. Cederbaum, and S. Fritzsche, Neon in ultrashort and intense x-rays from free electron lasers, J. Phys. B: At. Mol. Opt. Phys. **51**, 055602 (2018).

[26] K. Tiedtke, J. Feldhaus, U. Hahn, U. Jastrow, T. Nunez, T. Tschentscher, S. V. Bobashev, A. A. Sorokin, J. B. Hastings, S. Moeller, L. Cibik, A. Gottwald, A. Hoehl, U. Kroth, M. Krumrey, H. Schoeppe, G. Ulm, and M. Richter, Gas detectors for x-ray lasers, J. Appl. Phys. **103**, 094511 (2008).

[27] T. Maltezopoulos, F. Brinker, F. Dietrich, W. Freund, J. Grünert, U. F. Jastrow, N. Kujala, J. Laksman, J. Liu, K. Tiedtke, and T. Tschentscher, Hard x-ray operation of x-ray gas monitors at the European XFEL, J. Synchrotron Radiat. **31**, 681 (2024).

[28] P. Juranić, A. Alarcon, and R. Ischebeck, Online absolute calibration of fast FEL pulse energy measurements, J. Synchrotron Radiat. **30**, 500 (2023).

[29] H. Fukuzawa *et al.*, Deep inner-shell multiphoton ionization by intense x-ray free-electron laser pulses, Phys. Rev. Lett. **110**, 173005 (2013).

[30] Y. Kumagai *et al.*, Radiation-induced chemical dynamics in Ar clusters exposed to strong x-ray pulses, Phys. Rev. Lett. **120**, 223201 (2018).

[31] K. Toyota, Z. Jurek, S.-K. Son, H. Fukuzawa, K. Ueda, N. Berrah, B. Rudek, D. Rolles, A. Rudenko, and R. Santra, xcalib: A focal spot calibrator for intense x-ray free-electron laser pulses based on the charge state distributions of light atoms, J. Synchrotron Radiat. **26**, 1017 (2019).

[32] W. Jiang, X. Wang, S. Zhang, R. Dong, Y. Guo, J. Feng, Z. Shen, Z. Zhu, and Y. Jiang, A reaction microscope for AMO science at Shanghai Soft X-ray Free-Electron Laser Facility, Appl. Sci. **12**, 1821 (2022).

[33] W. Jiang, X. Wang, S. Zhang, R. Dong, Y. Guo, J. Feng, Z. Shen, T. Yan, Z. Zhu, and Y. Jiang, Dissociative multi-ionization of N_2O molecules in strong femtosecond laser field, J. Chem. Phys. **157**, 084302 (2022).

[34] R. Dong, A. Chen, J. Feng, S. Zhang, W. Jiang, X. Hu, Y. Wu, J. Wang, X. Wang, and Y. Jiang, Isomerization in highly excited states of triply charged carbon dioxide ions produced by intense laser fields, Phys. Rev. A **110**, 053110 (2024).

[35] P. Lablanquie, L. Andric, J. Palaudoux, U. Becker, M. Braune, J. Viefhaus, J. Eland, and F. Penent, Multielectron spectroscopy: Auger decays of the argon $2p$ hole, J. Electron Spectrosc. Relat. Phenom. **156–158**, 51 (2007).

[36] P. Lablanquie, M. Khalal, L. Andric, J. Palaudoux, F. Penent, J.-M. Bizau, D. Cubaynes, K. Jänkälä, Y. Hikosaka, K. Ito, K. Bucar, and M. Žitnik, Multi-electron coincidence spectroscopy: Triple Auger decay of Ar $2p$ and $2s$ holes, J. Electron Spectrosc. Relat. Phenom. **220**, 125 (2017).

[37] N. Rohringer and R. Santra, X-ray nonlinear optical processes using a self-amplified spontaneous emission free-electron laser, Phys. Rev. A **76**, 033416 (2007).

[38] S.-K. Son, L. Young, and R. Santra, Impact of hollow-atom formation on coherent x-ray scattering at high intensity, Phys. Rev. A **83**, 033402 (2011).

[39] C. Gao, J. Zeng, Y. Li, F. Jin, and J. Yuan, Versatile code DLAYZ for investigating population kinetics and radiative properties of plasmas in non-local thermodynamic equilibrium, High Energy Density Phys. **9**, 583 (2013).

[40] J. Zeng, P. Liu, W. Xiang, and J. Yuan, Level-to-level and total probability for Auger decay including direct double processes of Ar $2p^{-1}$ hole states, Phys. Rev. A **87**, 033419 (2013).

[41] P. Liu, J. Zeng, and J. Yuan, A practical theoretical formalism for atomic multielectron processes: Direct multiple ionization by a single Auger decay or by impact of a single electron or photon, J. Phys. B: At. Mol. Opt. Phys. **51**, 075202 (2018).

[42] L. Liu, Y. Li, C. Gao, and J. Zeng, Dominance of double processes in complete Auger decay of $Rb^+(3d^{-1})$, Phys. Rev. A **101**, 012507 (2020).

[43] Y. Li, C. Gao, J. Zeng, and J. Yuan, Effects of single-photon double photoionization and direct double Auger decay on K-shell ionization kinetics of Ar atoms interacting with XFEL pulses, J. Phys. B: At. Mol. Opt. Phys. **55**, 025002 (2022).

[44] See Supplemental Material at http://link.aps.org/supplemental/10.1103/j4rx-55m2 for theoretical results for ionization potentials and photoionization cross sections etc.

[45] M. Gu, The flexible atomic code, Can. J. Phys. **86**, 675 (2008).

[46] N. Saito and I. Suzuki, Multiple photoionization in Ne, Ar, Kr and Xe from 44 to 1300 eV, Int. J. Mass Spectrom. Ion Processes **115**, 157 (1992).

[47] S. Brünken, C. Gerth, B. Kanngießer, T. Luhmann, M. Richter, and P. Zimmermann, Decay of the $Ar2s^{-1}$ and $2p^{-1}$ and $Kr3p^{-1}$

and $3d^{-1}$ hole states studied by photoelectron-ion coincidence spectroscopy, Phys. Rev. A **65**, 042708 (2002).

[48] A. Müller, A. Borovik, T. Buhr, J. Hellhund, K. Holste, A. L. D. Kilcoyne, S. Klumpp, M. Martins, S. Ricz, J. Viefhaus, and S. Schippers, Observation of a four-electron Auger process in near-K-edge photoionization of singly charged carbon ions, Phys. Rev. Lett. **114**, 013002 (2015).

[49] S.-K. Son and R. Santra, Monte Carlo calculation of ion, electron, and photon spectra of xenon atoms in x-ray free-electron laser pulses, Phys. Rev. A **85**, 063415 (2012).

[50] J. Yan, G. Yan, F. Jin, Y. Li, C. Gao, J. Zeng, and J. Yuan, Evolution of level population in Ar interacting with XFEL pulses: Impact of resonant absorptions, J. Phys. B: At. Mol. Opt. Phys. **57**, 155601 (2024).